Available online at www.sciencedirect.com
SCIENCE DIRECT®
Journal of Magnetism and Magnetic Materials 288 (2005) 1–14
Journal of magnetism and magnetic materials
www.elsevier.com/locate/jmmm

A comparative three-dimensional neutron depolarization study on $RCrO_4$ oxides (R = Y, Er, Tm, Yb)

E. Jimenez-Melero[a,*], N.H. van Dijk[b], W.H. Kraan[b], P.C.M. Gubbens[b], J. Isasi[a], R. Saez-Puche[a]

[a]*Dpto. Quimica Inorganica, Fac. C. Quimicas, Universidad Complutense de Madrid, Ciudad Universitaria, 28040-Madrid, Spain*
[b]*Interfacultair Reactor Instituut, TUDelft, Mekelweg 15, 2629 JB Delft, Netherlands*

Received 28 May 2004; received in revised form 30 June 2004
Available online 4 August 2004

Abstract

Three-dimensional neutron depolarization experiments have been performed on $RCrO_4$ (R = Y, Er, Tm, Yb) powder samples in order to gain insight into their magnetic domain structure in the submicrometer range. The temperature evolution of both the average domain size and the net magnetization of each compound has been studied for different applied magnetic fields. The largest average domain size at zero external magnetic field was found in $YbCrO_4$. The effect of an applied magnetic field on the magnetic domain structure is relatively small in $ErCrO_4$ and $TmCrO_4$, when compared to $YCrO_4$ and $YbCrO_4$ where the average domain size even surpasses the average particle size determined by Scanning Electron Microscopy studies.

PACS: 75.30.Gw; 75.50.−y; 75.60.−d

Keywords: Rare earth chromates; Zircon-type structure; Magnetic anisotropy; Neutron depolarization; Magnetic domains

1. Introduction

$RCrO_4$ oxides (R = rare earth) are classified within the family of compounds of general formula RXO_4 (X = V, Cr, P, As). They crystallize into two different structural types: monazite (monoclinic symmetry, S. G. $P2_1/c$) or zircon (tetragonal symmetry, S. G. $I4_1/amd$), depending on the size of both the R(III) and the X(V) ions [1–3]. They have been subject to extensive studies concerning their optical and magnetic properties [4,5]. Rare earth chromates present two magnetic ions in the lattice, namely R(III) and Cr(V), so that they constitute an ideal tool to asses the nature of the magnetic 3d-4f interactions. The influence of

*Corresponding author. Tel.: +34-91-3944353; fax: +34-91-3944352.
E-mail address: ejmelero@quim.ucm.es (E. Jimenez-Melero).

0304-8853/$ - see front matter © 2004 Elsevier B.V. All rights reserved.
doi:10.1016/j.jmmm.2004.07.012

the Cr(V) ion on the overall magnetic properties can be unequivocally determined by comparison with the isostructural RXO_4 (X = V, P, As) oxides.

We have focused our study on the chromium derivates where R = Y, Er, Tm, and Yb. They all crystallize in the zircon-type structure, and the subtle changes in the lattice parameters are a direct consequence of the lanthanide contraction [2]. Therefore, differences in the magnetic properties among them are only due to the electronic configuration of the constituent ions. Ferromagnetic interactions have been reported at relatively low temperatures in these compounds, their ordering temperatures being 9 K ($YCrO_4$), 15 K ($ErCrO_4$), 18 K ($TmCrO_4$), and 25 K ($YbCrO_4$), respectively [6]. However, the latter shows an antiferromagnetic coupling of the magnetic moments of the Cr(V) and Yb(III) sublattices, leading to a ferrimagnetic structure [7].

The three-dimensional neutron depolarization technique yields information about magnetic inhomogeneities within the sample, whose mean magnetic correlation length lies in the micrometer range. In the case of the powdered $RCrO_4$ samples (R = Y, Er, Tm, Yb), magnetic domain structures are expected to form below the mentioned critical temperatures. Therefore, magnetic inhomogeneities arise from the different orientation of the local magnetic induction of the domains within the powder particles. The magnetization within each magnetic domain corresponds to the temperature-dependent saturation magnetization. We have performed a comparative study of the influence of the intrinsic magnetic anisotropy of the rare earth ions on the temperature and field evolution of the magnetic domains. In order to do so, $YCrO_4$ was chosen as a reference material, since there is no magnetic anisotropy coming from the Y(III) sublattice due to its diamagnetic character. Furthermore, the Cr(V) ion is considered to behave as magnetically isotropic, as deduced from its spectroscopic g-tensor [8].

2. Sample preparation and characterization

Powdered $RCrO_4$ samples were prepared using the corresponding nitrates as precursors, according to the following scheme [9]:

$$R(NO_3)_3 \cdot 6H_2O + Cr(NO_3)_3 \cdot 9H_2O \underset{853\,K}{\overset{O_2}{\rightleftarrows}} RCrO_4 + 15H_2O + 6NO_x.$$

Since the foregoing nitrates melt and subsequently decompose below 473 K, the reaction is actually taking place in the melt. The obtained green-colored samples were characterized by both X-ray and neutron diffraction [10]. The appearance of any secondary phase was not observed in either of the samples.

In a later stage, the four samples were studied by Scanning Electron Microscopy, in order to determine the particle size and its morphology. Similar results were obtained for all samples, which can be attributed to the fact that they present a similar composition (the same stoichiometry and only a change in the rare earth sublattice, the rare earth ions being chemically alike), the same crystallographic structure (only subtle changes in the lattice parameters due to the lanthanide contraction) and the same synthesis procedure. Fig. 1a displays the scanning electron micrograph of the $ErCrO_4$ sample. The particle sizes seem to be smaller than 1 μm, but the grains are forming agglomerates of sizes bigger than 1 μm. A subsequent Transmission Electron Microscopy study on samples obtained from suspensions ultrasonically dispersed under butanol revealed a particle size distribution of 0.1–0.5 μm, while confirming the zircon-type structure in these compounds. Fig. 1b shows the electron diffraction pattern of $ErCrO_4$ along the [0 1 0] zone axis. A few smaller particles of size between 0.05 and 0.1 μm were also present. Moreover, no grains composed of more than one crystallite were detected.

3. Three-dimensional neutron depolarization technique

3.1. Experimental details and theoretical considerations

In a three-dimensional neutron depolarization experiment, the change in the polarization vector

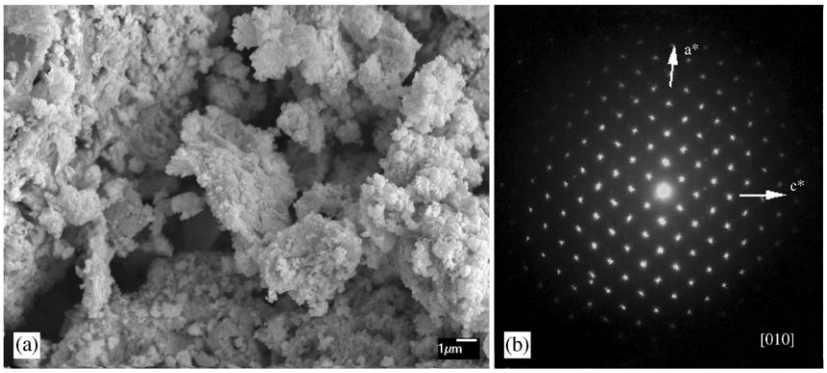

Fig. 1. (a) Scanning electron micrograph and (b) electron diffraction pattern along the [0 1 0] zone axis of the $ErCrO_4$ sample.

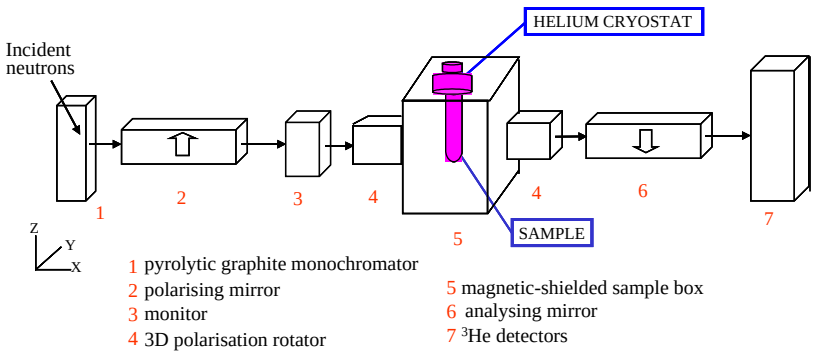

Fig. 2. Three-dimensional neutron depolarization set-up.

of a polarized neutron beam after transmission through the magnetic sample is analyzed. Such a change is characterized by a (3×3) depolarization matrix (**D**), according to the expression $\mathbf{P}' = \mathbf{D} \cdot \mathbf{P}$, where **P** and **P′** are the initial and final polarization vectors, respectively [11]. In order to obtain the nine elements of the depolarization matrix, one polarization rotator is placed before the sample and another one right after it. Each rotator provides the possibility to apply/analyze the polarization vector parallel or antiparallel to each of the coordinate axes x, y, z. Fig. 2 shows a sketch of the experimental neutron depolarization set-up. It is worth noting that the polarization direction transmitted by the analyzer is anti-parallel to that of the polarizer. The resultant neutron intensity is finally detected by two successive ^{3}He-filled detectors. The coordinate system we adopted is such that the x-direction coincides with the transmission direction of the neutron beam, the z-direction is parallel to the applied magnetic field, and the y-direction is perpendicular to the plane defined by both the x and z-directions. The polarization rotators enable to measure any matrix element D_{ij} in two complementary ways, delivering the intensities I_{ij} and I_{Ij}. Their average is denoted I_s. The matrix element D_{ij} is calculated according to

$$D_{ij} = (I_s - I_{ij})/I_s. \quad (1)$$

An amount of 600 mg of the powdered sample was introduced into a cylindrical volume with a diameter of 13 mm and a thickness of 3 mm, the latter being the transmission length of the neutron beam through the sample. The corresponding volume fraction (f_V) was 0.25 ($ErCrO_4$, $TmCrO_4$ and $YbCrO_4$) and 0.35 ($YCrO_4$), respectively. Afterwards, the powder was soaked with paraffin

to enhance the thermal contact between particles and with the sample holder, in order to effectively cool the sample and reach a homogeneous temperature within the sample. The intensity of the transmitted beam is reduced by a factor of 5 by soaking the powder sample in paraffin, due to incoherent scattering of the hydrogen. However, the reduction in intensity is independent of the polarization orientation of the neutron beam. Consequently, the reduction in intensity caused by the paraffin does not influence the measured polarization, but only its statistical accuracy.

A magnetic domain structure is expected to develop in these rare earth chromates below their magnetic ordering temperature. The polarized neutron beam is sensitive to the fluctuations in the local magnetic induction due to the presence of the magnetic domains, resulting in a shortening of the polarization vector. This phenomenon is reflected in the depolarization matrix, from which the correlation matrix α_{ij} (j referring to the incoming polarization direction and i the outgoing polarization direction) can be derived [12]. The correlation parameters α_{ij}, which contain the relevant information on the microscopic magnetic state of the sample, can be expressed as

$$\alpha_{ij} = \left\langle \int_0^{L_x} \Delta \mathbf{B}_i(x,y,z) \cdot \Delta \mathbf{B}_j(x+x',y,z)\mathrm{d}x' \right\rangle \quad (2)$$

where ΔB_i is the fluctuation of the local magnetic induction along the i-direction, $\langle \cdots \rangle$ represents a spatial average over the sample volume illuminated by the neutron beam, and L_x is the transmission length of the neutron beam through the sample (3 mm). When the magnetic domains are randomly oriented, the correlation matrix is diagonal. The trace of the correlation matrix then corresponds to the magnetic correlation function (ξ).

In these $RCrO_4$ compounds where ferro- or ferrimagnetic structures are present at low temperatures, ξ can be related to the average magnetic domain radius (R). From the determinant of the depolarization matrix, the magnetic correlation function can be deduced, according to the formula:

$$\det(\mathbf{D}) = \exp(-2cL_x\xi), \quad (3)$$

where $c = 2.15 \times 10^{29}\,\lambda^2\,\mathrm{T}^{-2}\,\mathrm{m}^{-4}$, with $\lambda = 0.2\,\mathrm{nm}$ (the neutron wavelength).

The three-dimensional neutron depolarization measurements also provide information about the mean-square direction cosines of the variation in local magnetic inductions along the three coordinate directions: γ_i [12]. They constitute a way to quantify the magnetic texture of the sample along the three orthogonal directions in space, and are related to the diagonal elements of the correlation matrix according to:

$$\gamma_i = \alpha_{ii}/\xi \quad (4)$$

The correlation parameters α_{ii} effectively describe the variation in the line integral along the neutron path of the magnetic induction oriented along the i-axis averaged over the cross-section of the beam. Therefore, the γ_i parameter probes which fraction of the total variation in the magnetic induction (caused by the magnetic domains present in the sample) is oriented along the i-axis.

When no external magnetic field is applied, the three components of the net magnetization are equal to zero within the sample, i.e. $\langle m_x \rangle = \langle m_y \rangle = \langle m_z \rangle = 0$, where $\langle m_i \rangle = \langle M_i \rangle / M_s$. In the absence of an average magnetic induction in the sample (for $\langle M \rangle = 0$), no net rotation of the polarization vector is obtained. However, when a magnetic field is applied, a net magnetization is developed along the direction of that applied field. Therefore, the polarization vector will rotate in the plane perpendicular to the net magnetization and, consequently, non-zero off-diagonal elements appear in the measured depolarization matrix. In our experiments, the applied magnetic field will be along the z-direction. In this case, information about the rotation experienced by the polarization vector can be obtained from the elements of the depolarization matrix, according to the expression:

$$\varphi = \arctan[(D_{xy} - D_{yx})/(D_{xx} + D_{yy})] \quad (5)$$

The polarization rotation is proportional to both the transmission length (L_x) and the net magnetization ($\langle M \rangle$):

$$\varphi = \eta c^{1/2} f_{\mathrm{M}} L_x \mu_0 \langle M \rangle \quad (6)$$

with f_M being the ferromagnetic volume fraction of the sample, and η being a geometrical factor to account for the influence of the stray fields caused by the magnetized sample. The product of the magnetic fraction (f_M) times the net magnetization ($\langle M \rangle$) and the constant μ_0 results in the net magnetic induction in the sample. Therefore, by the successive use of Eqs. (5) and (6), the induced net magnetization within the sample is obtained.

The temperature dependence of both the average magnetic domain size and the net magnetization in these $RCrO_4$ powdered samples was studied below their magnetic ordering temperature, both in zero field and in different applied magnetic fields. During the experiments, the samples were first cooled in zero field (ZFC) down to 2 K, subsequently warmed in an external magnetic field (FW) above the corresponding magnetic ordering temperature, and finally cooled (FC) in the same magnetic field down to 2 K. During these temperature scans, the nine elements of the depolarization matrix were continuously measured. The external magnetic field was generated by an aluminium coil placed around the cryostat. The maximum applied magnetic field was 8.0 mT. The time for each element to be measured varied from 5 to 15 s, depending on the measured signal (magnitude of depolarization) of each sample in order to get acceptable counting statistics. Measurements were also performed in zero field, both while warming (ZFW) and cooling (ZFC) the sample, so as to check if temperature hysteresis was present in any of the samples, and to subsequently assess the effect of the applied magnetic field on the average magnetic domain size.

3.2. Results and discussion

The changes in the nine elements of the depolarization matrix were studied for each sample as a function of temperature at different applied magnetic fields. The determinant of the depolarization matrix was normalized to its value at the highest measured temperature, well above the magnetic ordering temperature in all cases, so that the change in polarization could be ascribed to the magnetic domain structure within the sample. The rotation of the empty coil (obtained in the paramagnetic regime of the sample) was subtracted from the net rotation below the magnetic ordering temperature, so that only the net rotation caused by the sample magnetization induced by the applied magnetic field is probed. The wavelength of the monochromatic neutron beam was kept constant at $\lambda = 2.04\,\text{Å}$ throughout all experiments.

3.2.1. In the absence of an applied magnetic field

In Fig. 3, the experiments performed on the $YCrO_4$ sample are presented. When no external field is applied, all the off-diagonal elements of the depolarization matrix are equal to zero, implying that there are no correlations between the different directions of the local magnetic inductions. As a consequence, the determinant of the depolarization matrix is just the product of its three diagonal elements. A decrease in the determinant was found for $YCrO_4$ below 9 K, which confirms the previously reported value for its Curie temperature [6,13]. The determinant at 2 K only shows a small reduction and amounts to 0.988, as shown in the inset of Fig. 3. In general, the determinant below the Curie temperature reflects the temperature dependence of the saturation magnetization (M_S), the average domain radius (R) and the magnetic fraction (f_M). In this oxide, the decrease in the determinant with decreasing temperature mainly comes from the temperature dependence of the saturation magnetization (besides from a possible variation of the average domain size below the Curie temperature). Its magnetic fraction (f_M) corresponds to the volume fraction (f_V), which remains constant at all temperatures.

From the examination of the results for the three diagonal elements of the depolarization matrix in zero applied field, we infer that the magnetization directions of the different magnetic domains are isotropically distributed in the three directions of space. Consequently, a value of 1/3 is expected for the three average square components of the relative magnetization (i.e. $\langle m_x^2 \rangle = \langle m_y^2 \rangle = \langle m_z^2 \rangle = \frac{1}{3}$). In this situation, the mean-square direction cosines of the variation in the magnetic induction will take the values of

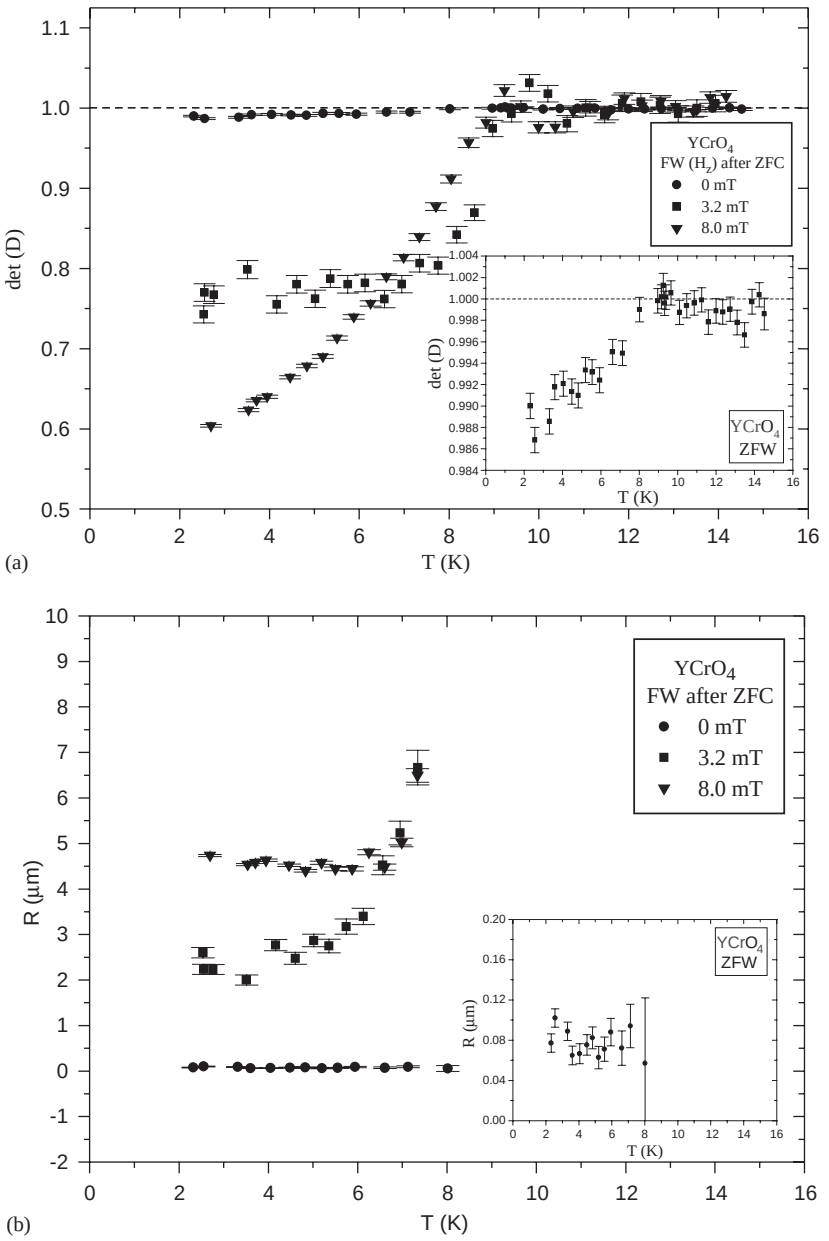

Fig. 3. Temperature dependence of (a) the normalized determinant and (b) the average domain radius of $YCrO_4$ during a field warming (FW) after zero-field cooling (ZFC) process, at different applied magnetic fields. The insets display the determinant and the average domain radius for zero-field warming (ZFW) respectively.

$\gamma_x = \frac{1}{2}, \gamma_y = \gamma_z = \frac{1}{4}$ [12]. We calculated the experimental γ_i coefficients for the measured depolarization matrix, according to the formula:

$$\gamma_i = 1 - 2\ln(D_{ii})/\ln(\det(\mathbf{D})) \quad (7)$$

This definition implies that their sum is equal to one. Surprisingly, we obtained the values of $\gamma_x \approx 0.4$ and $\gamma_y = \gamma_z \approx 0.3$. This difference may arise from the presence of some texture in the sample, or may be due to some orientational particle

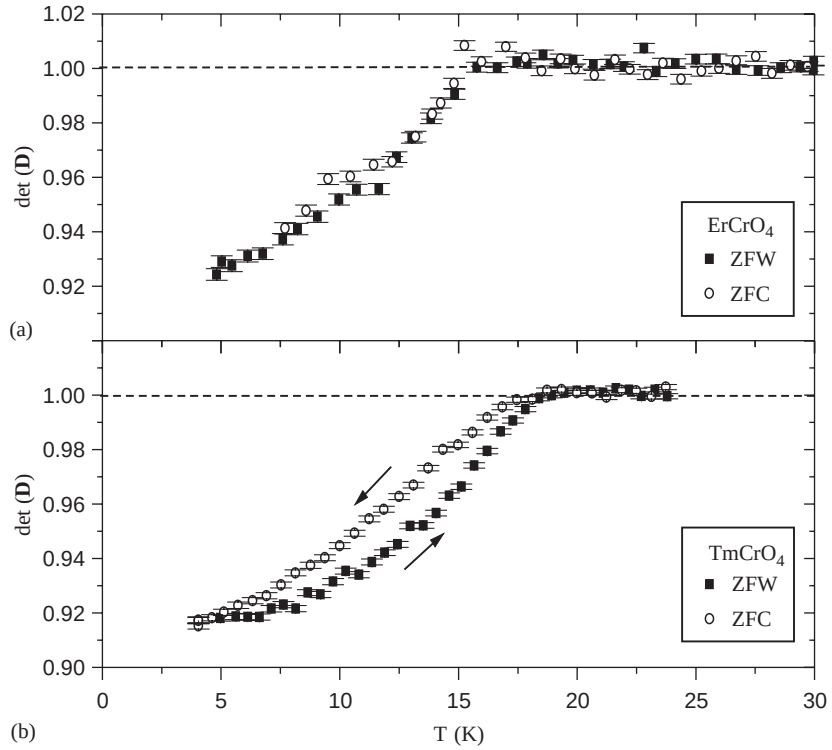

Fig. 4. Depolarization of the neutron beam det(**D**) in the magnetically ordered state during zero-field warming (ZFW) and cooling (ZFC) for (a) $ErCrO_4$ and (b) $TmCrO_4$. Note the influence of the first-order magnetic transition of the Tm(III) sublattice in $TmCrO_4$.

correlations when introducing the powder sample in the sample holder.

Subsequently, we performed similar experiments on the $ErCrO_4$, $TmCrO_4$ and $YbCrO_4$ samples. The temperature dependence of the determinant is displayed in Fig. 4 for $ErCrO_4$ and $TmCrO_4$ in the absence of an external field. While similar results were obtained in the case of $ErCrO_4$ and $YbCrO_4$ between zero-field cooling and warming, a clear temperature hysteresis was present in $TmCrO_4$ between its previously reported magnetic ordering temperature (18 K) and 6 K. The observed hysteresis is consistent with the presence of a first-order magnetic transition, which has just been reported between 18 and 8 K for $TmCrO_4$ by both ^{169}Tm Mössbauer spectroscopy and μSR measurements [14]. The Cr(V) sublattice fully orders ferromagnetically at 18 K, and seems to induce a magnetic moment in the Tm(III) crystal-field non-magnetic ground state. Below 8 K, 25% of the Tm(III) sublattice still remains paramagnetic. Even though the Tm(III) magnetic fraction varies notably with temperature, the Cr(V) sublattice is 100% magnetically ordered at 18 K. Hence, the magnetic fraction equals the volume fraction of the sample at all temperatures below 18 K. The magnetically ordered fraction of the Tm(III) sublattice will be reflected in the saturation magnetization at each temperature. In the case of the $YbCrO_4$ sample, no significant differences have been observed in the determinant between the ZFW and ZFC processes below 25 K. Moreover, the depolarization of the neutron beam is comparable to the one corresponding to the $YCrO_4$ sample. This similarity can be ascribed to the low values of the saturation magnetization in its ferrimagnetic state.

The determination of the average domain size from the measured determinant of the depolarization matrix requires that the saturation magnetization for each rare earth chromate as a function of

temperature is known. The saturation magnetization depends on the atomic structure and on the magnitude and orientation of the ordered magnetic moments on each sublattice. The magnetic structure of both $ErCrO_4$ and $TmCrO_4$ has recently been solved by powder neutron diffraction experiments [10]. In the former, the parallel magnetic moments of both sublattices lie in the basal plane, their ordered moments at 2 K being 5.09 μ_B and 0.91 μ_B for the Er(III) and Cr(V) ions, respectively. They yield a bulk magnetic induction of $\mu_0 M_S = 0.78$ T at 2 K. By contrast, the main ferromagnetic component in $TmCrO_4$ lies along the *c*-axis, corresponding to a value of $\mu_0 M_S = 0.52\,T$ at 2 K. The difference in orientation of the ordered magnetic moments between the $ErCrO_4$ and $TmCrO_4$ compounds seem to stem from the higher intrinsic magnetic anisotropy of the Tm(III) compared to the Er(III) ion, as deduced from its four times larger value of the second-order Stevens coefficient [15]. In the $YbCrO_4$ oxide, details about its ferromagnetic ordering have been recently derived from both bulk magnetization measurements and ^{170}Yb Mössbauer spectroscopy experiments [7]. The sublattice magnetizations, which are ferrimagnetically aligned with respect to one another, are 1.55 μ_B and 1 μ_B for Yb(III) and Cr(V) respectively, leading to a value of $\mu_0 M_S = 0.085$ T at 2 K. Even though the intrinsic magnetic anisotropy of the Yb(III) ion (its experimental spectroscopy *g*-tensor being $g_z = 5.8$ and $g_\perp = 1.1$) labels the *c*-axis as the easy axis of magnetization, the strongly anisotropic Yb–Cr magnetic interaction clamps the magnetic moments of both sublattices in the *ab*-plane. Finally, no detailed information about the magnetic structure of $YCrO_4$ is presently available. Bulk magnetization measurements reveal a saturation magnetization value of $\mu_0 M_S = 0.12$ T at 2 K. From the orientation of the ordered magnetic moments in the other three $RCrO_4$ oxides, we can infer that the magnetic moments in $YCrO_4$ are most likely oriented in the *ab*-plane.

Once the magnetic correlation function (ξ) has been obtained from the experimental values of the determinant of the depolarization matrix and Eq. (3), it can be subsequently used to derive the corresponding average magnetic domain radius. For spherical magnetic domains of radius R and a randomly oriented domain magnetization, the relevant relationship is [12]:

$$\xi = (1/2) f_M \mu_0^2 M_S^2 R. \tag{8}$$

This expression holds in the absence of an external magnetic field, or when $\mu_0\langle M\rangle \ll \mu_0 M_S$. Its modification to include texture effects with the anisotropy axis along the *z*-direction, as suggested by the experimental mean-square direction cosines, did not lead to a significant difference in the obtained values for the mean magnetic domain size (R) in either of the samples in the unmagnetized state. Therefore, the combination of Eqs. (3) and (8) allowed us to obtain mean magnetic domain size values at each temperature. In order to do so, the temperature dependence of the saturation magnetization is required. Subsequent experiments at different applied magnetic fields in field-cooling (FC) processes revealed that the net magnetization $\mu_0\langle M\rangle$, derived from the rotation of the polarization vector, is proportional to the external magnetic field at all temperatures. Consequently, we took $\mu_0 M_S(T)$ proportional to the mentioned rotation, normalized at 2 K to the values previously reported by neutron diffraction and/or bulk magnetization measurements. For instance, $\mu_0 M_S(T)$ for $ErCrO_4$ is displayed in Fig. 5b.

The values of the average magnetic domain size, calculated for temperatures between 2 K and $T_C/2$ (where T_C is the corresponding magnetic ordering temperature), for the different samples in the absence of an external magnetic field are collected in Table 1 ($YCrO_4$), and 2 and 3 ($ErCrO_4$, $TmCrO_4$, $YbCrO_4$), while its temperature dependence is shown in Fig. 3b ($YCrO_4$) and 6 ($TmCrO_4$), respectively. In all cases, the magnetic domain size remains constant with temperature, implying that the magnetic structure established right below the magnetic ordering temperature prevails down to 2 K. Only in $TmCrO_4$ slight differences are observed between field warming and cooling, probably arising from the first-order magnetic transition of the Tm(III) sublattice in the temperature range of 8–18 K. Surprisingly, $YbCrO_4$ presents the highest value of the average magnetic domain size, which is of the same order

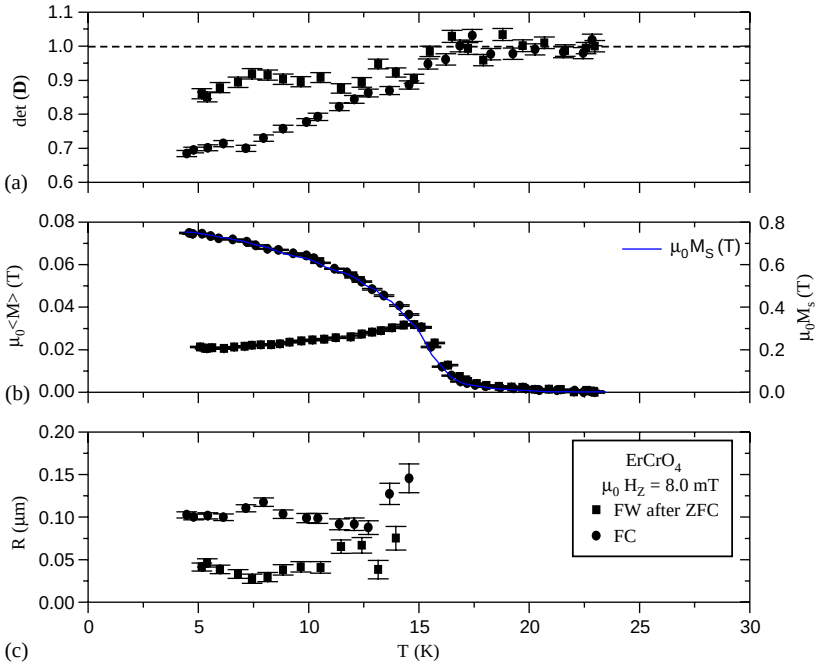

Fig. 5. Depolarization of the neutron beam caused by the $ErCrO_4$ sample when applying a magnetic field of 8.0 mT along the z-direction: (a) determinant; (b) net induced magnetization calculated from the observed rotation (left scale) and saturation magnetization (right scale); and (c) average magnetic domain radius.

Table 1
Average domain radius (μm) of $YCrO_4$ during both field warming after zero-field cooling (FW after ZFC) and field cooling (FC), calculated for temperatures between 2 K and $T_C/2$, where T_C is the corresponding magnetic ordering temperature

$\mu_0 H$ (mT)	FW after ZFC	FC
0	0.079(4)	0.079(3)
3.2	2.39(4)	3.75(6)
8.0	4.57(1)	4.58(1)

Table 2
Average domain radius (μm) of $ErCrO_4$, $TmCrO_4$ and $YbCrO_4$ during field warming (FW) after zero-field cooling (ZFC), calculated for temperatures between 2 K and $T_C/2$, where T_C is the corresponding magnetic ordering temperature

$\mu_0 H$ (mT)	$ErCrO_4$	$TmCrO_4$	$YbCrO_4$
0	0.021(1)	0.047(1)	0.350(7)
3.2	0.030(1)	0.056(2)	0.42(6)
6.4	0.035(2)	0.070(2)	0.58(7)
8.0	0.042(2)	0.071(1)	0.59(5)

of magnitude as the average particle size, as shown in the Tables 2 and 3. This fact indicates the existence of many single-domain particles. In the other remaining compounds, the deduced average domain size is lower than the particle size distribution, so that more than one magnetic domain must be present in each particle. But the average domain size is much larger than the lattice parameters, so that each magnetic domain comprises a significant number of unit cells (for instance, the lattice parameters for $TmCrO_4$ are: $a = 7.032(2)$ Å and $c = 6.181(9)$ Å [10]).

3.2.2. *In the presence of an applied magnetic field*

When we applied a magnetic field along the z-direction, a net magnetization is induced in the sample along that direction. The resultant non-diagonal depolarization matrix provides information about the rotation of the polarization vector,

Table 3
Average domain radius (μm) of $ErCrO_4$, $TmCrO_4$ and $YbCrO_4$ during field cooling (FC), calculated for temperatures between 2 K and $T_C/2$, where T_C is the corresponding magnetic ordering temperature

$\mu_0 H$ (mT)	$ErCrO_4$	$TmCrO_4$	$YbCrO_4$
0	0.019(1)	0.045(1)	0.368(7)
3.2	0.076(1)	0.367(3)	7.84(9)
6.4	0.085(2)	0.544(2)	8.79(6)
8.0	0.124(3)	0.631(1)	9.98(5)

together with its shortening due to the presence of the magnetic domain structure. The polarization rotation, directly obtained from the matrix elements using Eq. (5), is employed to infer the temperature dependence of the magnetization both in the field-warming after zero-field cooling and field-cooling processes. The shape factor (η) that accounts for stray fields comprises a macroscopic (η^M) and a microscopic (η^P) contribution, according to

$$\eta = (1 - f_M)\eta^P + f_M\eta^M \tag{9}$$

Both the microscopic factor for spherically shaped particles and the macroscopic factor for disc-like specimens take a value of $\frac{1}{2}$, so that in this case η also equals $\frac{1}{2}$ [16].

In the situation of a magnetized sample, the magnetic correlation function (ξ) can still be obtained from the determinant of the depolarization matrix (see Eq. (3)). However, the relationship between ξ and the average domain radius (R) should be modified, since a significant magnetization has been induced by the external magnetic field, especially in the field-cooling process. For a finite rotation around the z-axis and a low value of $\{f_M\langle m_z\rangle^2\}$, the expression to be used is [12]:

$$\xi = (3/(4\gamma_z + 5))f_M\mu_0^2 M_S^2 R. \tag{10}$$

The γ_z values at each temperature for a certain field process can be deduced from the D_{zz} element using Eq. (7), since that matrix element is not affected by the rotation of the polarization vector. The other two γ_i values cannot be obtained from a straightforward application of Eq. (7), due to the appearance of a cosine term that accounts for the rotation around the z-axis.

When the sample is magnetized by an applied magnetic field, the free poles that appear on its edges produces the well-known demagnetizing field (H_d) that is directed opposite to the net magnetization. It depends on the sample shape, and equals $H_d = -N\langle M\rangle$, where N is the demagnetizing factor. In the case of a powder sample, the magnetic fraction needs also to be taken into account when calculating H_d. Its causes the effective magnetic field inside the powder sample to be smaller than the applied magnetic field. For our powder samples which are placed inside a disc-like sample holder with a diameter of 13 mm and a width of 3 mm, the estimated demagnetizing factor is $N = 0.154$. The shape of the sample holder is approximated by a rotational ellipsoid [17]. It is worth noting that the applied magnetic field is oriented in the plane of the disc-shaped cylinder (along the diameter of 13 mm and perpendicular to the thickness of 3 mm).

Fig. 3 shows the variation in the determinant with temperature for $YCrO_4$ at different applied fields (field-warming after zero-field cooling) as well as in zero field, coupled with the corresponding values of the average domain size. When applying an external magnetic field at 2 K before warming the sample, a significant reduction of the determinant was clearly observed for increasing applied magnetic fields. As an example, a value of 0.600 was obtained at 2 K for a field of $\mu_0 H_z = 8.0$ mT, which constitutes a significant reduction from the value obtained in the absence of a magnetic field (of 0.988 at 2 K) (see inset of Fig. 3a). The mentioned large change in the determinant of $YCrO_4$ implies a remarkable increase in the average domain size. This effect points to weak magnetic exchange interactions within the Cr(V) sublattice. Comparatively, when the magnetic field is applied in the paramagnetic regime and the temperature is lowered (field-cooling process), the magnetization inside each particle can easily respond to that field due to the low magneto-crystalline anisotropy present right below the magnetic ordering temperature. As a consequence, the magnetic domains align their magnetization to the easy direction closest to the applied field direction, and a relatively large average domain size value is obtained. Table 1

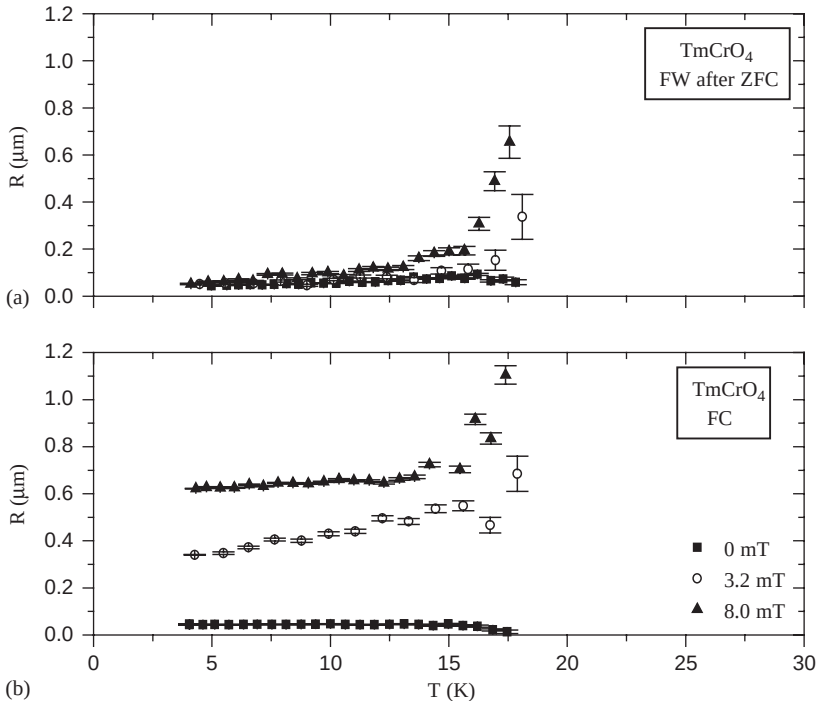

Fig. 6. Temperature dependence of the average domain radius of $TmCrO_4$ during (a) field warming after zero-field cooling (FW after ZFC) and (b) field cooling (FC).

represents the values of the average domain size of $YCrO_4$ for different fields and conditions. At a magnetic field of $\mu_0 H_z = 8.0\,\mathrm{mT}$, the value of the mean magnetic domain size is similar for both field-warming and field-cooling the sample. This similarity indicates that such a magnetic field is high enough to effectively activate the domain wall movement, even when the magnetic field is switched on at 2 K. This phenomenon is also reflected in the rotation values for both processes (see Fig. 7), where the remarkable differences that appear at a magnetic field of $\mu_0 H_z = 3.2\,\mathrm{mT}$ almost disappear at $\mu_0 H_z = 8.0\,\mathrm{mT}$. The latter field is high enough to magnetically saturate the sample even in field-warming.

The average domain size in $YCrO_4$ remains constant below the Curie temperature. However, the values obtained in the presence of a magnetic field exceed the mean particle size of 0.1–0.5 μm. This fact is indicative of clustering of neighbouring single-domain particles with their magnetizations directions aligned over the distance of the cluster size. In this situation, the neutron beam samples magnetic domains larger than the particle size. During these experiments the particles cannot rotate to align their magnetization with the field direction, because they are fixed within the paraffin. Furthermore, when approaching the Curie temperature while warming the sample in the presence of a magnetic field, a remarkable increase in the magnetic domain size is observed even reaching values of 7–8 μm, so that a significant amount of powder particles are clustered. This effect can be attributed to the low magneto-crystalline anisotropy right below the Curie temperature. In this $RCrO_4$ compounds, the magneto-crystalline anisotropy comprises a contribution for possible anisotropy effects in the R(III)–Cr(V) exchange interaction, and a contribution due to the intrinsic anisotropy of the constituent magnetic ions (only the R(III) ions in this case, since the Cr(V) ion is considered to be magnetically isotropic). None of these contributions are present in the $YCrO_4$ compound, so that

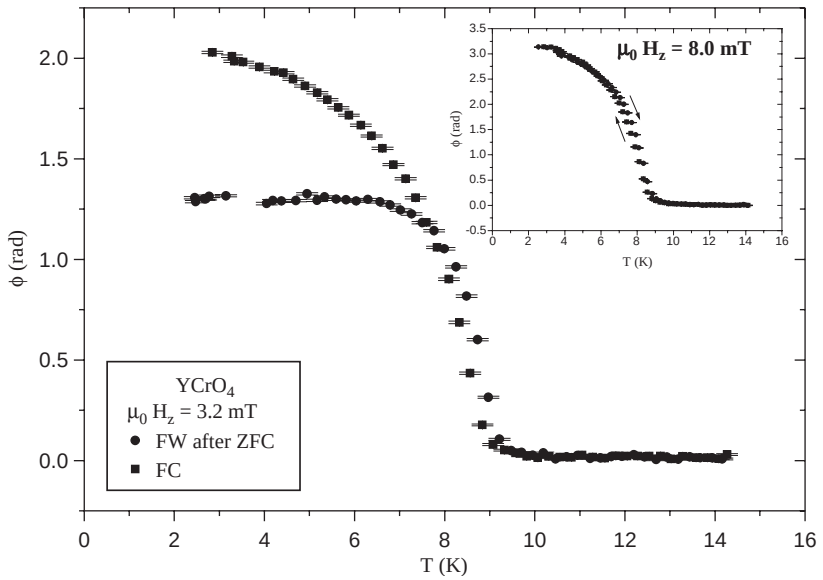

Fig. 7. Rotation of the polarization vector due to a net magnetization in $YCrO_4$ with an applied magnetic field of $\mu_0 H_z = 3.2$ and 8.0 mT (inset).

only the correlation between the particle shape and the orientation of the particle magnetization may hinder the alignment of the magnetizations of relatively big groups of particles along the direction of the applied magnetic field. Therefore, the $YCrO_4$ tends to present a phenomenon of magnetic percolation right below its magnetic ordering temperature. This effect appears when a certain concentration threshold is surpassed for different shapes of the magnetic particles [18–20]. A magnetic fraction of 0.35 seems to be high enough to permit the magnetic percolation to take place in the $YCrO_4$ sample. The presence of particle agglomerates also favors the detection of domain sizes bigger than the average particle size.

Subsequently, the values of the average domain size and the net magnetization were calculated for $ErCrO_4$ at different applied magnetic fields. Fig. 5 displays the results obtained for a magnetic field of $\mu_0 H_z = 8.0$ mT, while the values of the average domain size are collected in Tables 2 and 3 for different magnetic fields. There is a clear difference in the determinant of the depolarization matrix between field-warming and field-cooling the sample. The smaller values of the determinant in the latter process correspond to larger mean magnetic domain sizes. In both field histories, the calculated domain size remains constant within the experimental uncertainty below 15 K. This fact implies that the magnetic structure established when cooling below 15 K is not modified during cooling. The effect of the magnetic field is larger during field cooling, since the lower magneto-crystalline anisotropy right below the Curie temperature allows the magnetization in each magnetic domain to be better aligned with the external magnetic field [21]. Anyway, even with a magnetic field of $\mu_0 H_z = 8.0$ mT, the average domain size is smaller than the particle size distribution, which indicates that the majority of the particles are multi-domain. The value of $\mu_0\langle M\rangle = 0.08$ T at 4 K after the sample has been cooled in the presence of a magnetic field of $\mu_0 H_z = 8.0$ mT is just 15% of the saturation magnetization value at that temperature ($\mu_0 M_S = 0.52$ T). The magnetization shows a small increase during field-warming the sample after zero-field cooling, which can be ascribed to the concomitant reduction in the magneto-crystalline anisotropy close to T_C. All these results manifest the role that the Er(III) intrinsic magnetic anisotropy plays in hindering the possible magnetic domain growth caused by the application of

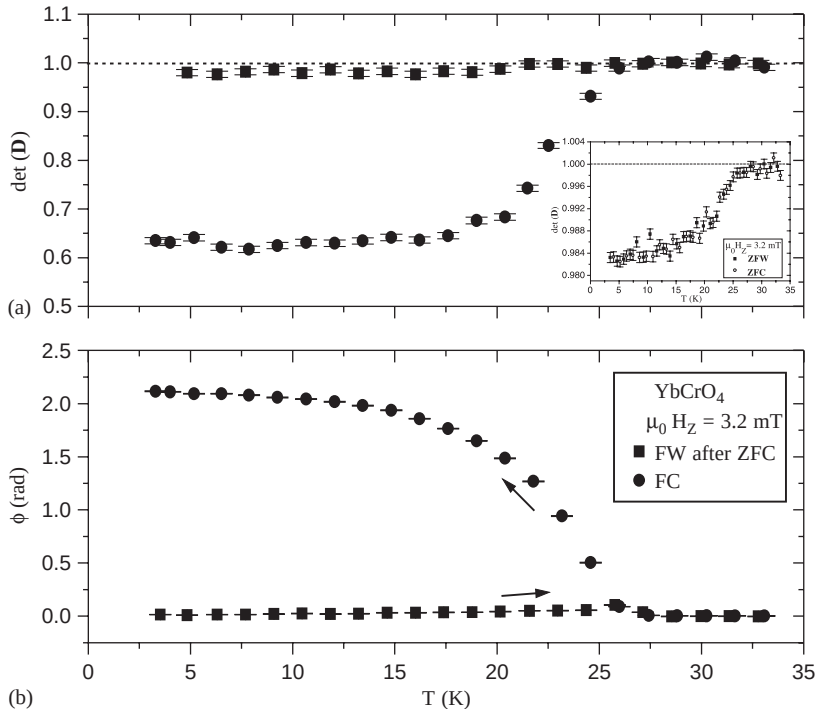

Fig. 8. Temperature dependence of the (a) normalized determinant and (b) net rotation of $YbCrO_4$ during field warming after zero-field cooling (FW after ZFC) and field cooling (FC) in an applied magnetic field of 3.2 mT. The inset of (a) corresponds to the normalized determinant during zero-field warming (ZFW) and zero-field cooling (ZFC).

an external magnetic field. The average magnetic domain size will change when the effect of the applied magnetic field is so large that some magnetic domains even grow at the expense of the disappearance of the smaller magnetic domains.

Fig. 6 shows the temperature dependence of the average domain size for the $TmCrO_4$ sample during the field warming after zero-field cooling and field cooling. The values of the magnetic domain size at 2 K are displayed in Tables 2 and 3, respectively. As in the other samples, higher values are obtained in the field-cooling process. In the latter, mean magnetic domain sizes comparable to the mean particle distribution are obtained even at an applied magnetic field of $\mu_0 H_z = 6.4$ mT. When decreasing the temperature in the presence of the applied magnetic field, a decrease in the average magnetic domain size is observed, which can be attributed to the progressive magnetic ordering of the Tm(III) whose intrinsic magnetic anisotropy can influence the magnetic domain structure a few degrees below the magnetic ordering temperature. Such magnetic ordering is also present during the field-warming process. However, there is a relatively large increase in magnetic domain size between 16 and 18 K, comparable to the one previously observed in the $YCrO_4$ sample. In that temperature region, only the isotropic Cr(V) ion is magnetically ordered. Therefore, it is possible to move magnetic domain walls to obtain single-domain particles and, subsequently to orient their magnetization along the field direction.

Finally, Fig. 8 shows both the determinant of the depolarization matrix and the rotation for $YbCrO_4$ in the presence of a magnetic field of $\mu_0 H_z = 3.2$ mT. No hysteresis has been observed in the determinant when no magnetic field is applied. Even though the reduction in the determinant is quite small (0.984 at 2 K), a mean magnetic domain size of 0.350(7) μm is obtained, due to the relatively small saturation magnetization of 0.085 T at 2 K in

this ferrimagnetic compound. Surprisingly, an applied magnetic field of only $\mu_0 H_z = 3.2\,\mathrm{mT}$ produces a substantial effect on the magnetic domain structure, especially in the field-cooling process. A value of 9.98(5) μm has been calculated for a magnetic field of $\mu_0 H_z = 8.0\,\mathrm{mT}$ at 2 K, which clearly exceeds the average particle size. In this compound, the anisotropy coming from the Yb(III)–Cr(V) magnetic exchange interactions appears to be much higher than the intrinsic magnetic anisotropy of the Yb(III) ion [7]. Moreover, its magnetic ordering temperature of 25 K is much higher than the one corresponding to the isostructural $YbVO_4$ oxide of only 93 mK [22]. This observation seems to be in line with the relatively high magnetic correlation length obtained by neutron depolarization experiments. Its estimated mean magnetic domain radius is significantly larger than the one observed in $TmCrO_4$ in the presence of the same external magnetic field, the main source of anisotropy in $TmCrO_4$ coming from the intrinsic anisotropy of the Tm(III) ion. While $TmCrO_4$ is mainly uniaxial, $YbCrO_4$ presents basal plane anisotropy. Hence it is easier to align the domain magnetizations under the influence of external magnetic fields in the latter compound.

4. Conclusions

Three-dimensional neutron depolarization experiments have allowed us to obtain information about parameters that characterize the magnetic structure of the $RCrO_4$ oxides in the submicrometer range, such us the average magnetic domain size and the magnetization. The temperature and magnetic field dependence of these parameters has been related to the possible sources of magnetic anisotropy within each sample. These experiments open the door to future similar studies on other ferro- or ferrimagnetic compounds that contain rare earth and/or transition metal ions.

Acknowledgements

The authors thank the MEC for financial support under the project MAT2003-08465-C02-01, and E. Urones and D. Avila from the Centro de Microscopia Luis Bru, UCM for their help in the Electron Microscopy study of the $RCrO_4$ samples.

References

[1] H. Schwarz, Z. Anorg Allg. Chem. 323 (1963) 44.
[2] G. Buisson, F. Bertaut, J. Mareschal, C. R. Acad. Sc. Paris 259 (1964) 411.
[3] B.C. Chakoumakos, M.M. Abraham, L.A. Boatner, J. Solid State Chem. 109 (1994) 197.
[4] G.A. Gehring, K.A. Gehring, Rep. Prog. Phys. 38 (1975) 1.
[5] G.J. Bowden, Aust. J. Phys. 51 (1998) 201 and references therein.
[6] H. Walter, H.G. Kahle, K. Mulder, H.C. Schopper, H. Schwarz, Int. J. Magn. 5 (1973) 129.
[7] E. Jimenez, P. Bonville, J.A. Hodges, P.C.M. Gubbens, J. Isasi, R. Saez-Puche, J. Magn. Magn. Mater. 272–276 (2004) 571.
[8] M. Greenblatt, J.H. Pifer, B.R. McGarvey, B.M. Wanklyn, J. Chem. Phys. 74 (11) (1981) 6014.
[9] E. Jimenez, M.J. Torralvo, J. Isasi, R. Saez-Puche, Chem. Educator 8 (1) (2003) 60.
[10] R. Saez-Puche, E. Jimenez, J. Isasi, M.T. Fernandez-Diaz, J.L. Garcia-Munoz, J. Solid State Chem. 171 (2003) 161.
[11] M. Rekveldt, Textures Microstruct 11 (1989) 127.
[12] R. Rosman, M. Rekveldt, J. Magn. Magn. Mat. 95 (1991) 319;
R. Rosman, M. Rekveldt, Phys. Rev. B 43 (10) (1991) 8437 and references therein.
[13] K. Tezuka, Y. Doi, Y. Hinatsu, J. Mater. Chem. 12 (2002) 1189.
[14] E. Jimenez, P.C.M. Gubbens, S. Sakarya, G.A. Stewart, P. Dalmas de Reotier, A. Yaouanc, J. Isasi, R. Saez-Puche, U. Zimmermann, J. Magn. Magn. Mater. 272–276 (2004) 568.
[15] K.N. Taylor, M.I. Darby, Physics of Rare Earth Solids, Chapman and Hall Ltd., London, 1972.
[16] N.H. van Dijk, S.G.E. te Velthuis, M.Th. Rekveldt, J. Sietsma, S. Van der Zwaag, Physica B 267–268 (1999) 88.
[17] S. Chikazumi, Physics of Ferromagnetism, 2nd edition, Oxford University Press, Oxford, 1999.
[18] J.-L. Mattei, O. Minot, M. Le Floćh, J. Magn. Magn. Mater. 140–144 (1995) 2189.
[19] M. Le Floćh, J.-L. Mattei, P. Laurent, O. Minot, A.M. Konn, J. Magn. Magn. Mater. 140–144 (1995) 2191.
[20] J.-L. Mattei, P. Laurent, O. Minot, M. Le Floćh, J. Magn. Magn. Mater. 160 (1995) 23.
[21] E. Jimenez, W.H. Kraan, N.H. Van Dijk, P.C.M. Gubbens, J. Isasi, R. Saez-Puche, Physica B 350 (1–3, Suppl. 1) (2004) E293.
[22] P. Radhakrishna, J. Hammann, P. Pari, J. Magn. Magn. Mater. 23 (1981) 254.